POLYMER MORPHOLOGY

Principles, Characterization, and Processing

EDITED BY
QIPENG GUO

WILEY

POLYMER
MORPHOLOGY

POLYMER MORPHOLOGY

Principles, Characterization, and Processing

Edited by

QIPENG GUO

WILEY

CONTENTS

16 Morphology Control of Polymer thin Films   **299**

Jiangang Liu, Xinhong Yu, Longjian Xue, and Yanchun Han

17 Polymer Surface Topography and Nanomechanical Mapping   **317**

Hao Liu, So Fujinami, Dong Wang, Ken Nakajima, and Toshio Nishi

18 Polymer Morphology and Deformation Behavior   **335**

Masanori Hara

PREFACE

Polymer morphology refers to the order within macromolecular solids and the structural constitution on the levels from nanoscale to a submicron and micron scale. The morphology plays an important role in the processing and application of polymeric materials. It embraces the processes of formation such as crystallization, deformation, and so on and the consequences for material properties as well as product performance.

Many books have been written on different particular aspects of polymer morphology. However, this book includes the basic principles and methods for morphological characterization, followed by a comprehensive understanding of polymer morphology, properties, and processing in a range of polymeric materials. It is composed of two parts: I. Principles and Methods of Characterization and II. Morphology, Properties, and Processing. Part I starts with an overview and prospects of polymer morphology, and then presents a detailed account of the principles and methods that are most used for investigation of polymer morphology. Morphology–property relationships are critical in the processing and applications of polymeric materials, which are addressed in Part II. The way in which the material is processed is a key determinant of the morphology and resulting properties. Understanding the morphology and the processes of its formation is essential in order to achieve the desired properties of a polymeric material in a certain application. A sampling of work in this area is also provided in Part II. I hope that it will not only serve as a useful textbook for advanced undergraduate and postgraduate students but also as a concise handbook for researchers in academia and engineers in related industries.

I express my appreciation and respects to all the contributors for their commitment, patience, and cooperation. Finally, I wish to express my sincere gratitude to the staff of John Wiley & Sons, Inc., especially Jonathan T. Rose who invited me to edit this comprehensive book and provided helpful support, and also Purvi Patel and Amanda Amanullah for her assistance during the edition.

Qipeng Guo
2015
Australia

LIST OF CONTRIBUTORS

Ruth Cardinaels, Department of Chemical Engineering, KU Leuven, 3001 Leuven, Belgium

Pierre J. Carreau, Chemical Engineering Department, Ecole Polytechnique de Montreal, Montreal H3T 1J4, Canada

K. L. A. Chan, Department of Chemical Engineering, Imperial College London, London SW7 2AZ, UK

Peng Chen, Department of Materials, School of Chemistry and Chemical Engineering, Anhui University, Hefei, 230039, China

Sossio Cimmino, Istituto per i Polimeri, Compositi e Biomateriali, Consiglio Nazionale delle Ricerche, 80078, Pozzuoli, Italy

M.-B. Coltelli, Department of Civil and Industrial Engineering, University of Pisa, 56126, Pisa, Italy

Duraccio Donatella, Istituto per i Polimeri, Compositi e Biomateriali, Consiglio Nazionale delle Ricerche, 80078, Pozzuoli, Italy; Istituto per le Macchine Agricole e Movimento Terra (IMAMOTER) – Consiglio Nazionale delle Ricerche, Torino, 10135, Italy

So Fujinami, RIKEN SPring-8 Center, RIKEN, Hyogo 679-5148, Japan

Abbas Ghanbari, Chemical Engineering Department, Ecole Polytechnique de Montreal, Montreal H3T 1J4, Canada

G. Groeninckx, Department of Chemistry, Division of Molecular and Nanomaterials, Laboratory of Macromolecular Structure Chemistry, Katholieke Universiteit Leuven, 3001 Heverlee, Belgium

Jean-Michel Guenet, Institut Charles Sadron, CNRS-Université de Strasbourg, 67034 Strasbourg, France

Qipeng Guo, Institute for Frontier Materials, Deakin University, Geelong, Victoria, 3220, Australia

Yanchun Han, State Key Laboratory of Polymer Physics and Chemistry, Changchun Institute of Applied Chemistry, Chinese Academy of Sciences, Changchun, 130022, China

Masanori Hara, Department of Chemical and Biochemical Engineering, Rutgers University, Piscataway, NJ 08854-8058, USA

Charef Harrats, Laboratoire de Chimie Appliquée (LAC), DGRSDT, Institut des Sciences et Technologie, Ctr Univ Belhadj Bouchaib, Ain Temouchent 46000, Algeria

Xuehao He, Department of Chemistry, School of Science, Tianjin University, Tianjin, 300072, China

Marie-Claude Heuzey, Ecole Polytechnique de Montreal, Montreal H3T 1J4, Canada

Wenbing Hu, Department of Polymer Science and Engineering, School of Chemistry and Chemical Engineering, Nanjing University, Nanjing 210093, China

S. G. Kazarian, Department of Chemical Engineering, Imperial College London, London SW7 2AZ, UK

Werner Lebek, Institute of Physics and Institute of Polymeric Materials, Martin Luther University Halle-Wittenberg, 06099 Halle, Germany

Xuejin Li, Division of Applied Mathematics, Brown University, Providence, RI 02912, USA

Hao Liu, Zhengzhou University, Zhengzhou, 450001, China

Jiangang Liu, State Key Laboratory of Polymer Physics and Chemistry, Changchun Institute of Applied Chemistry, Chinese Academy of Sciences, Changchun, 130022, China

Arnaldo T. Lorenzo, The Dow Chemical Company, Performance Plastics R&D, Freeport, TX 77541, USA

Antonella Marra, Istituto per i Polimeri, Compositi e Biomateriali, Consiglio Nazionale delle Ricerche, 80078, Pozzuoli, Italy

Hironori Marubayashi, Department of Organic and Polymeric Materials, Graduate School of Science and Engineering, Tokyo Institute of Technology, Tokyo 152-8552, Japan

Rose Mary Michell, Grupo de Polímeros USB, Departamento de Ciencia de los Materiales, Universidad Simón Bolívar, Apartado 89000, Caracas 1080-A, Venezuela

Goerg H. Michler, Institute of Physics and Institute of Polymeric Materials, Martin Luther University Halle-Wittenberg, 06099 Halle, Germany

Paula Moldenaers, Department of Chemical Engineering, KU Leuven, 3001 Leuven, Belgium

Alejandro J. Müller, POLYMAT and Polymer Science and Technology Department, Faculty of Chemistry, University of the Basque Country UPV/EHU, Paseo Manuel de Lardizabal 3, 20018. Donostia-San Sebastián, Spain; IKERBASQUE, Basque Foundation for Science, 48013 Bilbao, Spain; Grupo de Polímeros USB, Departamento de Ciencia de los Materiales, Universidad Simón Bolívar, Apartado 89000, Caracas 1080-A, Venezuela

N. Sanjeeva Murthy, New Jersey Center for Biomaterials, Rutgers University, Piscataway, NJ 08854, USA

Ken Nakajima, Department of Organic and Polymeric Materials, Graduate School of Science and Engineering, Tokyo Institute of Technology, Tokyo 152-8550, Japan

Toshio Nishi, International Division, Tokyo Institute of Technology, Tokyo 152-8550, Japan

Shuichi Nojima, Department of Organic and Polymeric Materials, Graduate School of Science and Engineering, Tokyo Institute of Technology, Tokyo 152-8552, Japan

Anbazhagan Palanisamy, Institute for Frontier Materials, Deakin University, Geelong, Victoria, 3220, Australia

Marilena Pezzuto, Istituto per i Polimeri, Compositi e Biomateriali, Consiglio Nazionale delle Ricerche, 80078, Pozzuoli, Italy

Holger Schönherr, Department of Chemistry – Biology, Physical Chemistry I, University of Siegen, 57076 Siegen, Germany

Jerold M. Schultz, Department of Chemical Engineering, University of Delaware, Newark, DE 19716-3110, USA

Anne Seidlitz, Department of Physics, Martin-Luther University Halle-Wittenberg, 06120 Halle, Germany

Clara Silvestre, Istituto per i Polimeri, Compositi e Biomateriali, Consiglio Nazionale delle Ricerche, 80078, Pozzuoli, Italy

Xiaoli Sun, State Key Laboratory of Chemical Resource Engineering and Beijing Key Laboratory of Membrane Science and Technology, Beijing University of Chemical Technology, Beijing 100029, China

Thomas Thurn-Albrecht, Department of Physics, Martin-Luther University Halle-Wittenberg, 06120 Halle, Germany

Minh-Tan Ton-That, Automotive and Surface Transport, National Research Council Canada, Ottawa, K1V 1S2, Canada

Hiroki Uehara, Department of Chemistry and Chemical Biology, Gunma University, Gunma 376-8515, Japan

Dong Wang, State Key Laboratory of Organic-Inorganic Composites, College of Materials Science and Engineering, Beijing University of Chemical Technology, Beijing 100029, China

Longjian Xue, Dynamic Biointerfaces, Max Planck Institute for Polymer Research, Mainz, 55128, Germany

Takeshi Yamanobe, Department of Chemistry and Chemical Biology, Gunma University, Gunma 376-8515, Japan

Shouke Yan, State Key Laboratory of Chemical Resource Engineering and Beijing Key Laboratory of Membrane Science and Technology, Beijing University of Chemical Technology, Beijing 100029, China

Xinhong Yu, State Key Laboratory of Polymer Physics and Chemistry, Changchun Institute of Applied Chemistry, Chinese Academy of Sciences, Changchun, 130022, China

Liyun Zha, Department of Polymer Science and Engineering, School of Chemistry and Chemical Engineering, Nanjing University, Nanjing 210093, China

PART I

PRINCIPLES AND METHODS OF CHARACTERIZATION

1

OVERVIEW AND PROSPECTS OF POLYMER MORPHOLOGY

JEROLD M. SCHULTZ

Department of Chemical Engineering, University of Delaware, Newark, DE, USA

1.1 INTRODUCTORY REMARKS

Why are we interested in the morphology of polymers? I would like to say that our interest is in the inherent beauty and intriguing complexity of the patterns. Two examples are microphase-separated block copolymers and homopolymers crystallized from the melt. Figure 1.1 shows the range of morphologies typical to simple AB copolymers [1]. These structures are defined by the composition of the diblock copolymer: alternating plates for approximately equal amounts of components A and B, proceeding through double gyroid, rod, and sphere morphologies as the composition is made increasingly unbalanced (see Chapters 10, 14, and 15). More complicated repetitive morphologies are found in more complex block systems [1, 2]. Importantly, the repetition scales of these morphologies are of the same order as the dimensions of the molecular coils of the blocks – typically, tens of nanometers. Homopolymers crystallized from the melt display morphological features from the micrometer range to tens of nanometers. Figure 1.2 is an optical micrograph of spherulites of poly(ether ketone ketone) crystallizing from the melt. Seen in the figure are arms radiating from a central point, the arms then branching at small angles, to fill all space between the arms. Higher resolution images reveal that the arms are composed of stacks of long, ribbonlike crystals, with the molecules running in the thin direction of the crystals, as sketched in Figure 1.3 [3]. Why and how did such long-chain molecules, very highly intertangled in the melt, disentangle themselves to form this spherically symmetric array of bundles of lamellar crystals?

Certainly, the beauty of and the desire to understand the complexity of systems such as block copolymers and melt-crystallized polymers have played a role in driving the study of morphology. But most of the research in this area is funded and executed because properties of the polymeric materials are tied to the morphological detail. For instance, the fine-scale repetitive morphology of block copolymers makes them well suited for photonics [4], as well as for photovoltaic [5, 6] and battery [7] applications. Figure 1.4 shows a recent result for a block copolymer used as a photovoltaic system. The block copolymer is poly(3-hexylthiophene)–*block*–poly((9,9-dioctylfluorene)-2, 7-diyl-alt-[4,7-bis(thiophen-5-yl)-2,1,3-benzothiadiazole]-2′, 2″-diyl) (P3HT-*b*-PFTBT), with a composition of 56 wt% P3HT. With nearly equivalent volume fractions of each block, the system has an alternating plate morphology, as shown in Figure 1.4a. The *I–V* curve shown at the right demonstrates an efficiency of about 3%. While this efficiency is not competitive with current commercial photovoltaics, it is encouraging for the earliest stages of a new approach.

While the study of the morphology of polymers has been an occasional topic for over a century, it became a field of study in its own right with the advent of commercial transmission electron microscopes some 60 years ago. It was only then that the fine structures unique to polymers could be resolved and directly observed. But the electron beam in electron microscopies typically destroys the specimen in a few tens of seconds, precluding much in the way of following the evolution of fine morphological detail. Studies of morphological evolution were based on less direct (but
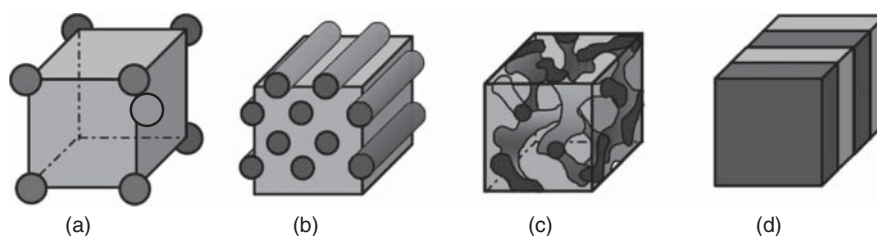
Figure 1.1 Morphology of AB diblock copolymers. From (a–d), in increasing composition from 0 to 50 vol%, spheres arranged on a body-centered cubic lattice, hexagonally packed cylinders, gyroid, and lamellae. Balsara and Hahn [1]. Reproduced with permission of World Scientific.
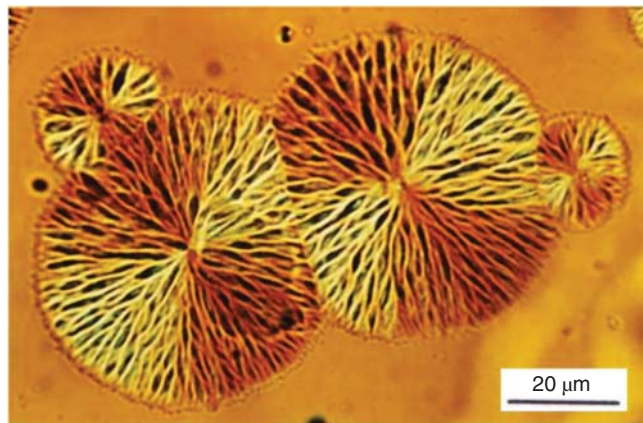
Figure 1.2 Spherulites growing into a melt of poly(ether ketone ketone) (PEKK 70/30, a copolymer of 70% terephthalate and 30% isophthalate moieties) at 280 °C.
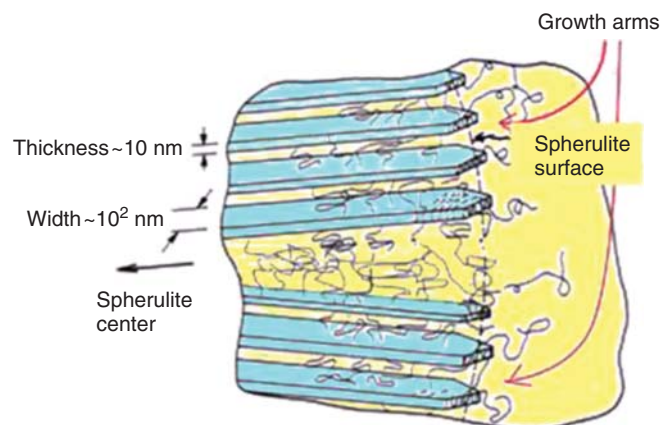
Figure 1.3 Sketch of a growing spherulite, showing crystalline lamellae and growth arms (stacks of lamellae). Schultz [3]. Reproduced with permission of American Chemical Society.

nonetheless useful) scattering, diffraction, spectroscopic, and calorimetric methods, in which local structure was educed from bulk behavior. This situation changed in the late 1990s with the advent of scanning probe microscopies and, somewhat more recently, with imaging based on spectroscopies. The current state of structural tools is detailed in Chapters 2–9 of this book.

1.2 EXPERIMENTAL AVENUES OF MORPHOLOGICAL RESEARCH

There are broadly three avenues of investigation of morphology. One is the characterization of the morphological state of a polymeric material. All of Part 1 and parts of Part 2 of this book deal specifically with characterization. As mentioned, there would be no need for a science of polymer morphology, were the morphology unimportant in establishing properties. Morphology–property relationships are then a second important area of study. A sampling of recent morphology–property research is given in Chapters 18 and 21, with examples included in other chapters. The third avenue is the study of how processing controls morphological detail, and hence also defines the behavior of the product. A sampling of work in this area is provided in Chapters 11–16, 19, 20, and 22. The three avenues of research are treated in the following subsections.

1.2.1 Morphological Characterization: The Enabling of *in situ* Measurements

Because so much of this compilation is already devoted to characterization, we concentrate here on only two aspects: rapid measurements and combined techniques.

One of the most interesting developments over the few decades of morphological study has been the development of tools for following morphological development *in situ* during processing operations. Many of these *in situ* methods awaited the development of fast measurement tools. Synchrotron radiation has provided X-ray and infrared (IR) intensities orders of magnitude higher than had been possible in laboratory-scale instruments. This beam intensity, plus the creation of detectors capable of capturing an entire spectrum of data in parallel, has reduced scan times for individual measurements from the order of an hour to the order of milliseconds. The technologies that enabled such work were the development of one- [7, 8] and two-dimensional [9, 10] position-sensitive wire detectors in the 1970s and of polymer-oriented beamlines at synchrotrons, beginning in the mid-1980s [11]. In parallel, more recently, Chase and Rabolt have similarly provided a rapid advance for infrared spectroscopy, developing a parallel capture system [12–14]. Another pair of important breakthroughs in the first decade
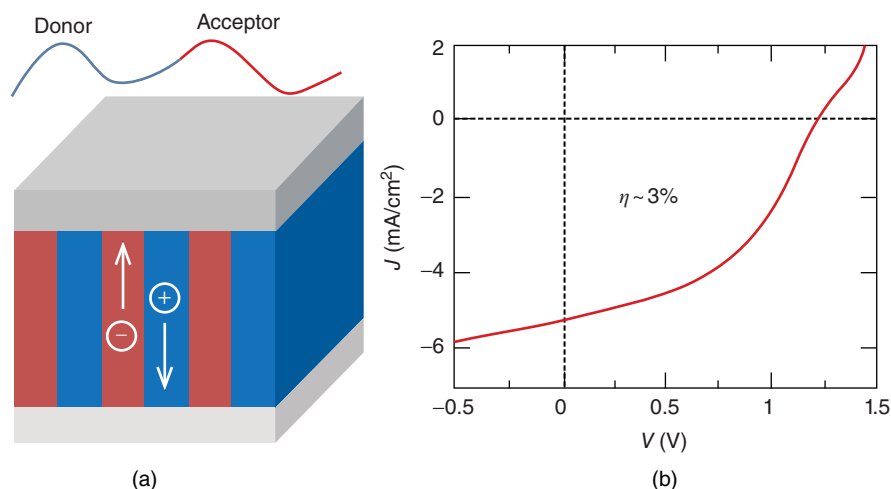
Figure 1.4 (a) Sketch of alternating lamellar morphology of a photovoltaic device made from the block copolymer poly(3-hexylthiophene)–block–poly((9,9-dioctylfluorene)-2,7-diyl-alt-[4,7-bis(thiophen-5-yl)-2,1,3-benzothiadiazole]-2′,2″-diyl) (P3HT-*b*-PFTBT), with a composition of 56 wt% P3HT. (b) *I–V* curve for the device. Guo et al. [6]. Reproduced with permission of American Chemical Society.

of the 2000s were the recognition that morphological development from the melt could be followed at high resolution by atomic force microscopy (AFM) [15–17], and the subsequent development of a very fast method of obtaining AFM images [18–21]. Using AFM, the same area can be probed many times at high resolution, in contrast to the situation for electron microscopies.

Another area of recent advances is in imaging using signals other than light, electrons, or neutrons. Scanning microscopies have enabled the use of any of a wide variety of signals, among which are surface friction (AFM phase mode), near-field optics, time-of-flight secondary ion mass spectroscopy (ToF-SIMS), and infrared and Raman absorption. An example of ToF-SIMS mapping across a spherulite, from Sun et al. [22], is shown in Figure 1.5. Seen is a map of the positions from which molecular fragments representing poly(ethylene oxide) (PEO) and poly(L-lactic acid) (PLLA) occur in a ring-banded spherulite of a 50/50 blend of PEO and PLLA. This image shows a radially periodic alternation of the two components. The periodic alternation is as yet unexplained. Figure 1.6, from Cong et al. [23], shows IR images taken at three different times during the growth from the melt of an isotactic polypropylene (iPP) spherulite at 142 °C. The band at 1303 cm^{-1} represents crystalline iPP; the band at 998 cm^{-1} represents ordered sequences of iPP in the melt. The spatial disposition of the 998 cm^{-1} band demonstrates the preordering of iPP chains in the melt ahead of the spherulite front. IR imaging is described in detail in Chapter 7.

1.2.2 Morphology–Property Investigation

An ongoing example of correlating morphology and properties is that of the mechanical behavior of engineering polymers. In the case of tensile deformation, one ideally follows changes in
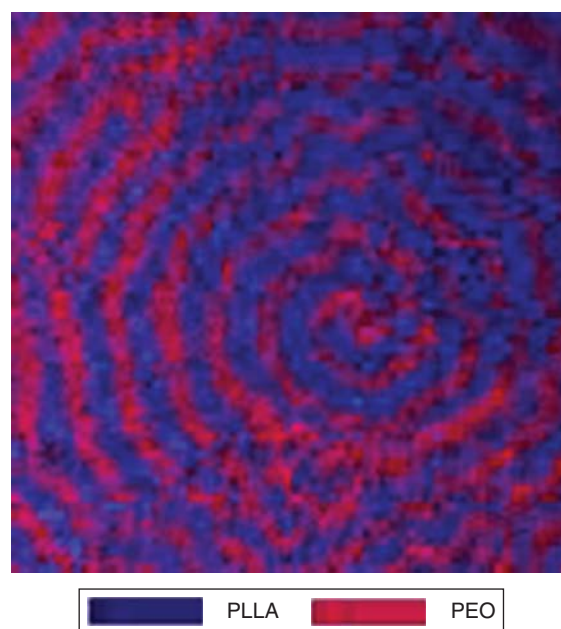
Figure 1.5 An ion map of a banded spherulite that formed in a 3-μm-thick film of a PLLA/PEO (50/50) blend crystallized between a silicon wafer and a Kapton cover for 5 h at 125 °C. Image obtained after removal of the Kapton. Sun et al. [22]. Reproduced with permission of Elsevier.

structure at the intermolecular, lamellar, and spherulite levels. Optical microscopy and small-angle light scattering can be used to follow spherulite-level changes during deformation, while wide-angle and small-angle X-ray scattering are available for intermolecular and lamellar study, respectively. Infrared absorption can be used to follow molecular-level changes. Until relatively recently, only light scattering has been fast enough to follow events *in situ* during deformation.
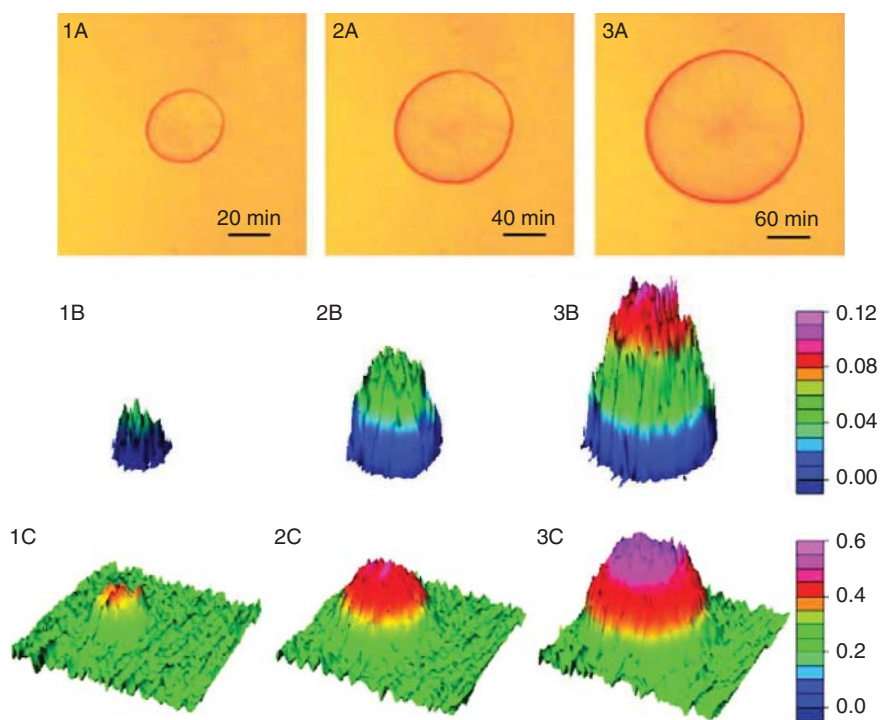
Figure 1.6 *In situ* optical microscope images of a single spherulite (set A) and the corresponding 3D images of intensity distribution of different conformational bands. Sets B and C refer to 1303 and 998 cm^{-1} bands, respectively. 1−3 are collected at different times during isothermal crystallization at 142 °C. The scale bar is 50 μm. Cong et al. [22]. Reproduced with permission of American Chemical Society.
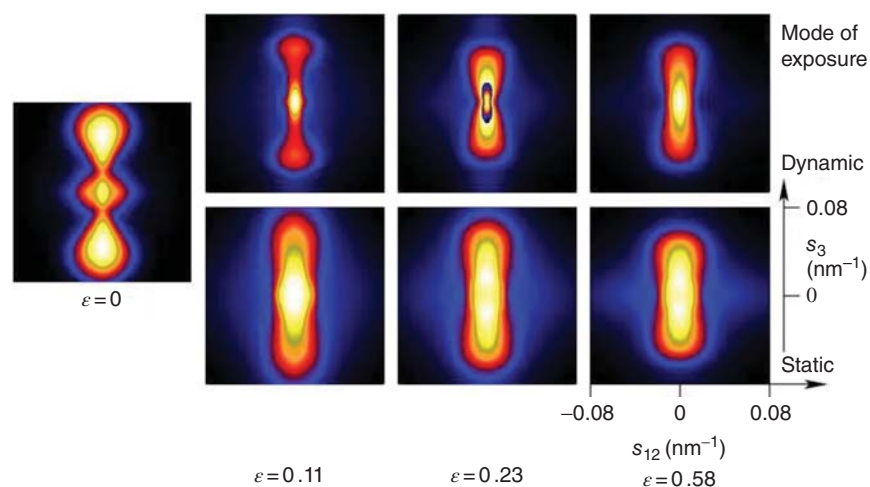
Figure 1.7 SAXS patterns obtained during tensile testing of oriented iPP films. Straining direction is vertical. Top row: during continuous straining at 10^{-3} s^{-1}. Bottom row: stretch-hold method. Stribeck et al. [31]. Reproduced with permission of John Wiley and Sons.

Optical microscopy [24, 25] and light scattering [26] studies in the 1960s showed clearly that spherulites underwent large-scale deformation as entities. In this earlier work, a specimen was extended a certain amount and then held there until a measurement was made (over several minutes) and then extended to the next level (*stretch-hold* investigation). But polymer spherulites are composed of ribbonlike crystals, with intervening layers of uncrystallized material. How does this finer structure deform so as to allow spherulites to change

shape, and how are these mechanisms reflected in stress–strain behavior? To address these questions, tensile deformation devices were built onto laboratory-scale X-ray systems, and small- and wide-angle X-ray scattering (SAXS and WAXS) patterns sampled during interruptions of deformation, again each pattern requiring several minutes [27, 28]. A good deal was learned about intraspherulitic deformation mechanisms: sequentially, deformation of the amorphous layer, shear of lamellae along the chain axis, and destruction of lamellae,
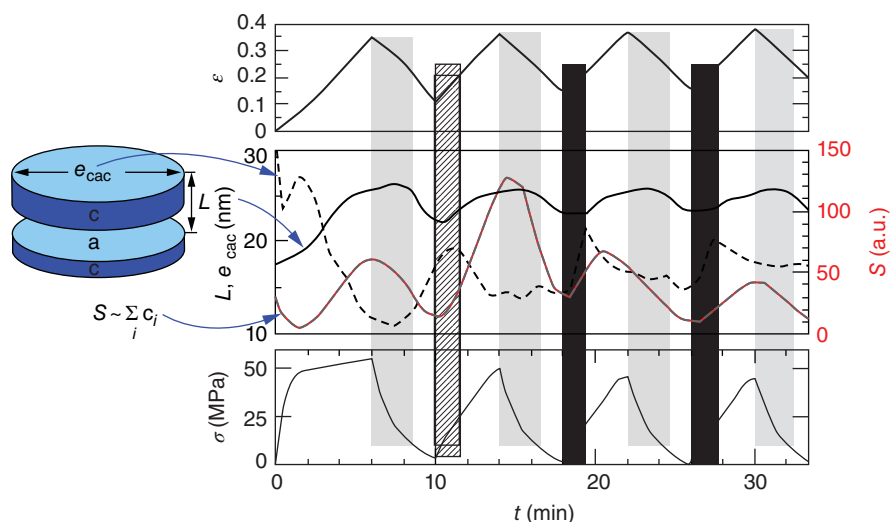
Figure 1.8 Dynamic load-reversal mechanical test of hard-elastic iPP film at a strain rate of $\dot{\varepsilon} \approx 10^{-3}$ s^{-1}. The following are shown as a function of elapsed time t: top – elongation; middle – long period L (solid line), lateral extension of a sandwich made of two crystalline lamellae (broken line), and strength of the chord distribution function (dotted line); bottom – tensile stress. Vertical bars indicate zones of strain-induced crystallization (black) and relaxation-induced melting (gray). Stribeck et al. [32]. Reproduced with permission of John Wiley and Sons.

followed later by the creation of fibrils [29] along the stress direction (see Ref. [30] for a review of the earlier work).

While this older work provided glimpses of mechanisms, the studies were problematic in two major ways. First, there was considerable relaxation of the system during the time in which measurements were taken. This has been brought home recently in parallel synchrotron-based studies of the same polymer deformed according to the older stretch-hold procedure and by continuous drawing [31]. Results are shown in Figure 1.7. The difference between the stretch-hold SAXS patterns (top) and the continuous deformation patterns (bottom) are large, and show broadly that the perfection of the lamellar stacks increased considerably during the hold period. In most studies reported in the past 15–20 years, SAXS and WAXS data was collected during continuous deformation. The results relate to intermolecular strain (WAXS) and lamellar deformation (SAXS). An example of such results for cyclic loading and unloading of a hard elastic iPP film is shown in Figure 1.8 [32]. It is interesting that the strength of the SAXS signal S rises and falls with the applied strain, apparently showing alternating crystallization and melting. Excellent descriptions of experimental methods and devices for synchrotron studies of mechanical behavior are found in Refs [33] and [34].

Fairly recently, IR measurements have been combined with mechanical testing and synchrotron X-rays, providing additional information on changes within the chain [35]. Finally, microbeam synchrotron X-ray investigation has permitted the study of structural variations at different positions within a specimen, for instance, skin versus core in fibers [36].

It should be mentioned that the spherulite size itself can be important in the failure behavior of spherulitic polymers. Some early literature in this area can be found in Refs [37] and [38].

An interesting finding is reported by Sandt [39]. In this work, it was shown that the mode of crack propagation gradually changed from interspherulitic to intraspherulitic with increasing rate of deformation, as shown in Figure 1.9.

1.2.3 Morphology Development

1.2.3.1 Flow-Induced Crystallization In most polymer processing, the material is highly stretched in the melt while it crystallizes. The most extreme cases of such processing are in fiber spinning and film blowing. In the case of the spinning of poly(ethylene terephthalate) (PET) fibers from the melt, stretch rates of the order of kilometers per minute are typical, and crystallization rates can be increased by some five orders of magnitude in melt-oriented fibers, relative to the quiescent state [40]. The final state of melt-spun PET fibers is that of row structures: stacks (rows) of thin lamellar crystals with the chain axis aligned along the thin dimension of the lamellae and along the fiber axis [41]. It had long been conjectured that these lamellae nucleated on very fine precursor fibrils, and it was suspected that the fibrillar precursors were either present only ephemerally or were hidden by the prolific overgrowth of lamellar crystals. Ephemeral precursory fibrils (with diameters of a few nanometers) were identified, using transmission electron microscopy (TEM) [42, 43] and also by performing radial distribution function analysis [42] (two very difficult experiments!) in fibers crystallized in the solid state after quenching to an oriented, noncrystalline structure. But the study of the early stages of crystallization during actual spinning operations awaited the construction of the spinning apparatus at synchrotron sites. The early stages are now well documented, including the initial precursor fibrils and the subsequent growth of lamellae. This work has been reviewed by Somani et al. [44].
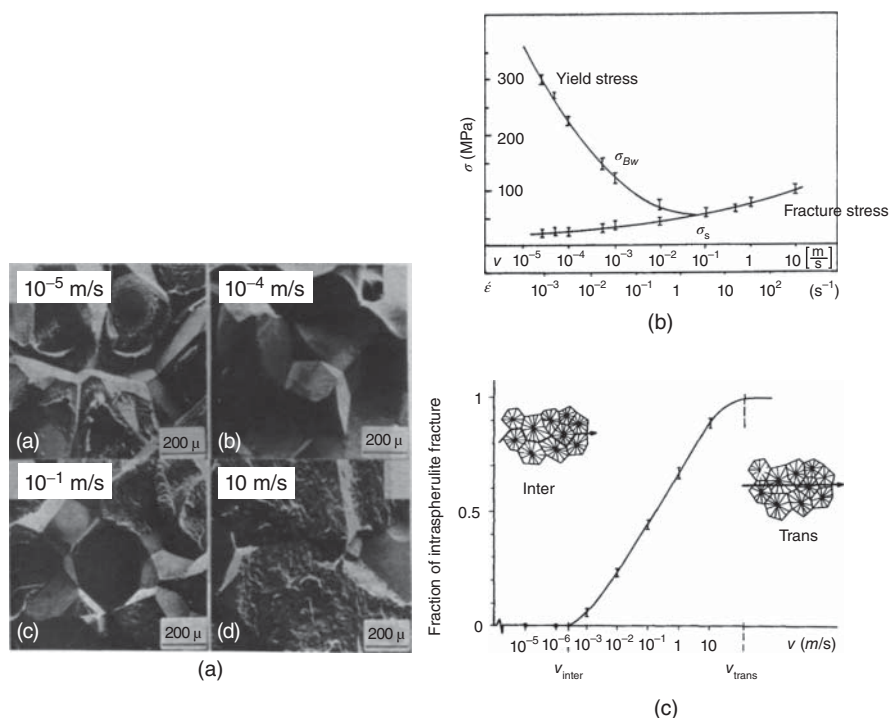
Figure 1.9 Effect of strain rate on the fracture of spherulitic iPP: (a) Scanning electron micrographs of the fracture surface, in which fracture along interspherulite boundaries is seen at the three lowest strain rates, while intraspherulite fracture is seen at 10 m/s; (b) yield stress and fracture stress versus strain rate; (c) fraction of intraspherulite fracture versus strain rate. Sandt [39]. Reproduced with permission of Ruhr-Universitaet Bochum.

It is relatively easy to build heaters and other ancillary equipment in the spacious and accessible specimen area at synchrotron beamlines. Consequently, the synchrotron-based study of morphological development during crystallization from the melt is now nearly routine. Similarly, deformation devices, with heaters attached, are found at synchrotron polymer beamlines, and numerous synchrotron-based reports of morphological development during drawing can be found.

1.2.3.2 Spherulite Formation It has been recognized for almost 60 years that polymer spherulites are composed of ribbonlike lamellar crystals in which the chains lie parallel to the thin direction and must reenter each crystal numerous times (see, e.g., Ref. [45], for an excellent early review). The most interesting phenomena occur at the level of individual lamellae, and until relatively recently sufficiently high resolution has been available only in electron microscopy. Because of the low specimen life in an electron beam, and because of the usual use of irrecoverable staining or etching, electron microscope study of the fine structure of spherulites has been limited to "post mortem" observation, at room temperature, of fully crystallized material. Some of the most detailed and careful TEM studies have been performed by Bassett and coworkers, using etching methodologies. The earlier work in this laboratory is reviewed in Refs [46] and [47]. In this work, done primarily on polyethylene and polypropylene, it was found that spherulites develop through the growth first

of individual primary lamellae, with backfilling by secondary lamellae. It was also shown that, at least some of the time, lamellar twist occurred discretely, rather than continuously. More recent work, using AFM, has been able to follow the fine-scale development of spherulites *in situ* (see Ref. [48] for a recent review).

While it is the time-lapse sequences that are unique, "still" shots during transformations are also instructive. Examples are shown in Figures 1.10 and 1.11. Figure 1.10, taken during the early stages of growth of a spherulite of PBA-C8 (a poly(bisphenol A octane ether)) shows the transition from a single lamella to a spherulite, via small-angle branching [50]. Figure 1.11 shows the growth front of a poly(caprolactone) spherulite. Evident are the spade-like tips of the lamellae and the cloning of lamellae in a stack by growth about giant screw dislocations [49].

1.3 MODELING AND SIMULATION

In the past two to three decades, quantitative modeling of morphogenesis has shifted significantly from analytical theory to numerical simulation. Although the facile use of analytical expressions in engineering application is valuable, the ability of numerical simulation to predict details of morphological development has opened new paths of understanding. Two areas in which our understanding has been moved forward are (i) numerical simulations of polymer phase separation and
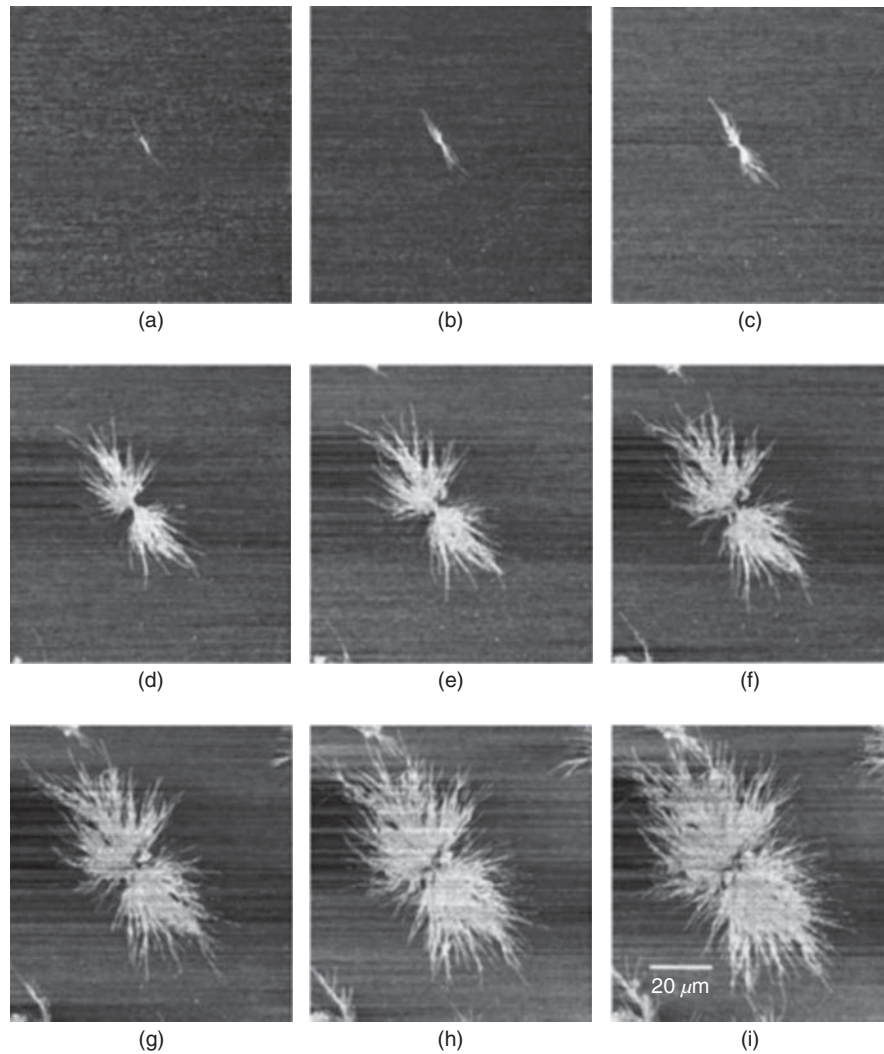
Figure 1.10 AFM phase images of spherulite development in PBA-C8. The temperature was 30 °C and the overall time was 167 min. Lei et al. [50]. Reproduced with permission of Elsevier.

crystallization and (ii) analyses of the roles of self-generated fields in polymer crystallization. Simulations are nicely covered in Chapters 13 and 15 and are not treated further here.

1.3.1 Self-Generated Fields

As a crystallization front progresses into a melt, three kinds of fields are formed in the melt ahead of the front. First, because of the density difference between crystal and melt and the slow stress relaxation in the viscous melt, a pressure or stress field is set up, with a gradient of negative pressure decreasing in magnitude with the distance from the interface. Second, the latent heat of fusion is continuously released at the crystallization front, resulting in a thermal field highest at the interface and decreasing into the melt. If there exist in the melt molecular species that cannot crystallize, or crystallize slowly in the propagating crystals, these species are excluded from the crystal and must diffuse away, down a composition gradient, into the melt. This "solute" buildup and its gradient

constitute a third type of self-generated field, a compositional field. These fields are characterized by a diffusion length $\ddot{o}$. δ is the distance from the interface at which the field strength (temperature, pressure, or impurity composition) has dropped from its value f_i at the solid/melt interface to a level $(f_i - f_o)/e$ above the far-field value f_o (i.e., the far-field value plus $1/e$ of the difference between the built-up value at the interface and the far-field value). For thermal and compositional fields, $\ddot{o} = D/V$, where D is the thermal or mass diffusivity and V is the velocity of propagation of the solid/melt interface. For a pressure field, $\delta_P = \frac{D_{self}}{V} = \frac{\beta}{\eta V}$, where D_{self} is the self-diffusivity of chains in the melt, η is the melt viscosity, and β is the Einstein equation coefficient, relating diffusivity and viscosity. High levels of temperature, pressure, or impurities in the melt at the interface act to slow the velocity of the interface. A very small diffusion length indicates that the field level is high at the interface. The interface propagation velocity V is set by the undercooling $T_m^o - T_c$, where T_m^o is the equilibrium melting point and T_c is the crystallization
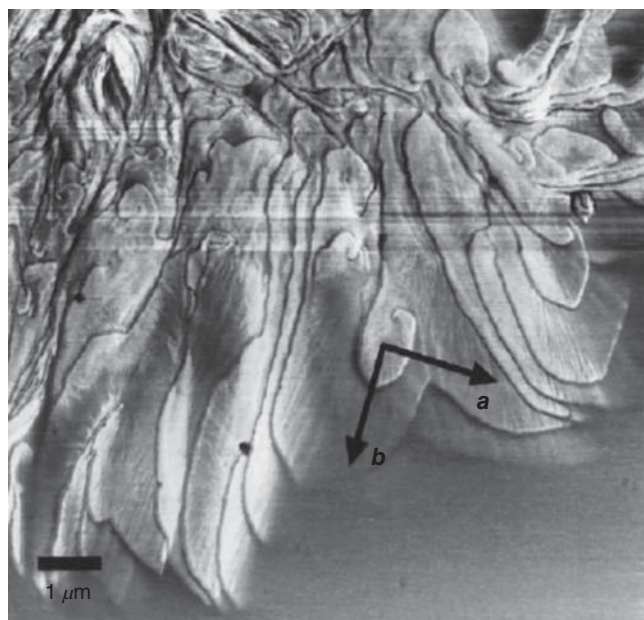
Figure 1.11 AFM image of a larger PCL structure grown at 57 °C from a molten film. Spiral growths from giant screw dislocations are abundant in views that are intermediate between flat-on and edge-on. Beekmans and Vancso [49]. Reproduced with permission of Elsevier.

temperature. The interface velocity increases steeply with the undercooling. The buildup of stress, heat, or uncrystallizable material (solute) at the interface all act to decrease the equilibrium melting point, thereby decreasing the V. For a smooth, continuous interface (a plane or a sphere), buildup continues as the front propagates, slowing the motion of the front continuously. The velocity decreases with time t, proportionally to $t^{-1/2}$ [51]. Thermal diffusivity is relatively very high, and consequently the thermal diffusion length is almost always very large, rendering heat buildup at the interface negligible. Thermal effects can be ignored. (The only possible exception is for the very high values of interface velocity associated with the spinning or heat treating of melt spun fiber [52, 53].)

The reasons that self-generated pressure or compositional fields are morphologically important is that the buildup of stress or impurities is greatly diminished if growth occurs as a fine needle or ribbon, because the stress or impurities at the tip can then be dissipated in three dimensions, as opposed to one-dimensional flow for a large flat or spherical surface. The growing body then adjusts its fineness to match the rate of dissipation with the rate of growth. In this context, then, the width of crystal lamellae and the size of stacks of lamellae could be governed by stress or compositional fields, and indeed finite-element [54] and analytical [55] modeling show this to be the case. A finite element result representing the growth-front propagation in a 50/50 blend of syndiotactic (crystallizable) and atactic (not crystallizable) polystyrene (iPS and aPS) is shown in Figure 1.12. In this example, a stack of ribbonlike lamellae of small thickness and infinite width is made to propagate forward in fine growth steps. At each growth step, the diffusion equation is solved locally in front of each lamella, and also the stack is made to increase by one new crystal (simulating spawning by a giant screw dislocation). The lamellar crystal grows at the velocity dictated by the instantaneous composition in the melt at the growth front. Shown in Figure 1.12 are the front positions after 20, 40, 60, 80, and 100 growth increments. One sees the formation of a narrow growth arm propagating linearly with time into the melt. Most of the uncrystallizable polymer has diffused laterally and produces a large interface composition in front of the lamellae at the sides of the growth arm. The growth front of these lamellae at either side propagates at a velocity proportional to $t^{-1/2}$. For these "secondary," trailing lamellae, the solute or pressure can be dissipated only normal to the front, whereas at the growth arm tip these can be dissipated laterally, as well as forward. This change in the dimensionality of the field is important and allows a constant growth velocity for the arm. The absolute growth arm diameters given by this method are in broad agreement with measurement for the iPS/aPS system [54, 55].

Another area in which self-generated field studies has been useful is in the crystallization from miscible blends in

Figure 1.12 Computed growth front after 20, 40, 60, 80, and 100 steps. Parameters match a 50/50 iPS/aPS blend crystallizing into the melt at 260 °C. Kit and Schultz [54]. Reproduced with permission of John Wiley and Sons.

Figure 1.13 Phase field simulations of the growth of a spherulite. Upper row: composition maps. A grayscale map was used to increase the contrast. Lower row: orientation map. Schultz [56]. Reproduced with permission of American Physical Society. (*See color plate section for the color representation of this figure*)
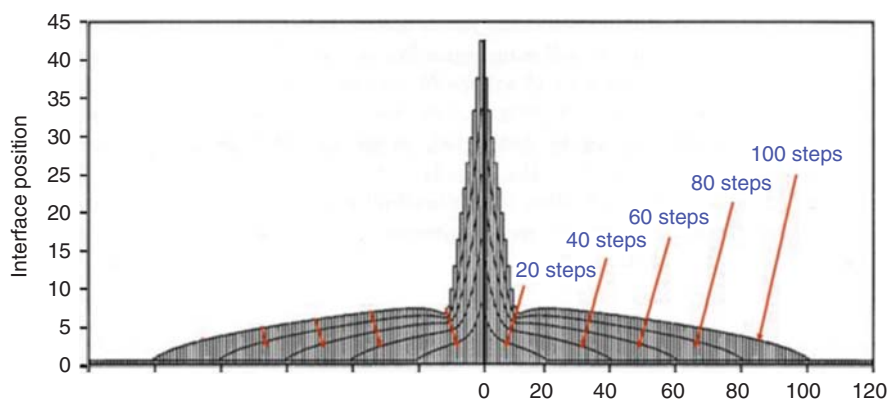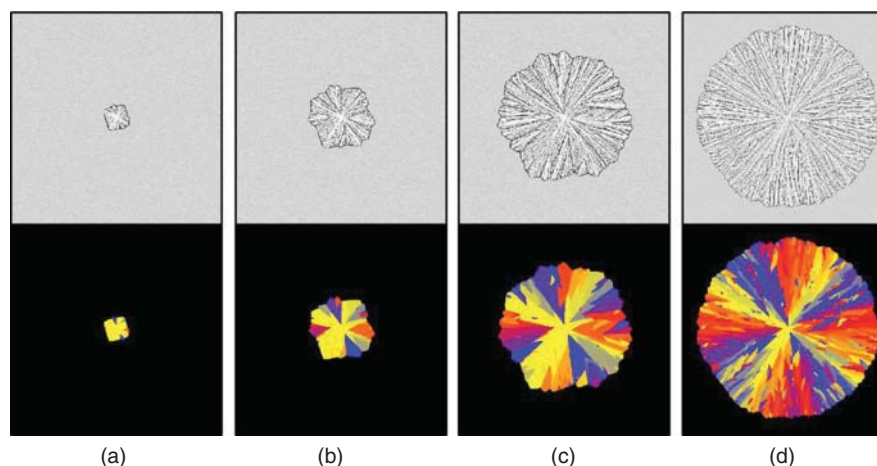
which only one component crystallizes (or crystallizes first). In these systems, the noncrystallizing component can reside finally between crystalline lamellae, between growth arms, or between spherulites. Selection from these possibilities is governed by the magnitude of the diffusion length. A review of this area can be found in Ref. [56].

This topic has also been approached by phase-field modeling. Phase-field modeling is an elegant approach for following the propagation of a front at a fine scale, in the presence of self-generated fields. In this method, equations representing the local evolution of order (crystallinity) and the local transfer of heat or chemical species are coupled. The order parameter is allowed to vary continuously from a crystalline phase (value 1) to a noncrystalline phase (value 0), over a very short distance (the "interface thickness"). The order parameter is related to the local entropy, and use is made of equilibrium and irreversible thermodynamics formalisms. Phase-field modeling applied to two-dimensional spherulitic polymer crystallization produces time-lapse images of the growing spherulite and can replicate known features of spherulitic growth [57–59]. Figure 1.13 is an example of the phase-field simulation of the growth of a spherulite in a blend. Most of the important features are captured, but the relationships to real-life conditions (particularly temperature) are not available. The current weakness in the phase-field modeling of polymer crystallization is that the coupling of growth kinetics and front propagation does not yet have the steep temperature dependence of front propagation which is experimentally known, the argument being made that only a more simplified coupling can allow simulation to be carried out in reasonable time.

1.4 WISHFUL THINKING

I have no crystal ball and am not endowed with second sight; I cannot predict the future. I comment here only on what I

perceive to be useful. Certainly the ultimate aim of all polymer morphology research is to produce useful products. In order to engineer such products, one would like to schedule a sequence of processes whereby a morphology is created suitable to the end use of the product. In polymer processing, this is almost always done by "feel," with the connections of processing to morphology and morphology to property not fully made. In other areas of materials science – think, for instance, of solid-state devices and of steels and cast irons – these connections have been made, and processing to achieve specific end uses is done with significantly better quantitative understanding. In the case of polymers, much greater effort has been made in characterizing morphology than in putting processing–morphology and morphology–property relations on a strong, quantitative footing. Advances in measurement technology and simulation methods have now put us in position to perform the studies that will make possible the detailed, quantitative processing–morphology and morphology–property connections. It is hoped that more effort will be placed in these areas, in both academia and industry, with profitable interactions between the two.

1.5 SUMMARY

The ultimate goal of morphology research is in the end product. Work in this area can be divided into the areas of morphology characterization, processing–morphology relationships, and morphology–property relationships. Recent advances in characterization tools have allowed measurements, at appropriate accuracy, to be made orders of magnitude faster than was previously possible. Further, microscopic mapping of properties such as IR absorption and viscosity are now available. These tools are enabling *in situ* studies of the development of morphology and the correlation of morphology with properties. Examples of synchrotron X-ray investigation of morphological development in fiber

spinning and of the changes of morphology with mechanical behavior are given. It is hoped that such studies will place the engineering of polymer products on an improved quantitative footing.

REFERENCES

1. Balsara N, Hahn H. Block copolymers in nanotechnology. In: Yong P, editor. *The Chemistry of Nanostructured Materials*. Singapore: World Scientific Publishing Co; 2003. p 317–327.

2. Abetz V, Simon PFW. Phase behaviour and morphologies of block copolymers. Adv Polym Sci 2005;189:125–212.

3. Schultz JM. Self-generated fields and polymer crystallization. Macromolecules 2012;45:6299–6323.

4. Darling SB. Block copolymers for photovoltaics. Energy Environ Sci 2009;2:1266–1273.

5. Orilall MC, Wiesner U. Block copolymer based composition and morphology control in nanostructured hybrid materials for energy conversion and storage: Solar cells, batteries, and fuel cells. Chem Soc Rev 2011;40:520–535.

6. Guo C, Lin Y-H, Witman MD, Smith KA, Wang C, Hexemer A, Strzalka J, Gomez ED, Verduzco R. Conjugated block copolymer photovoltaics with near 3% efficiency through microphase separation. Nano Lett 2013;13:2957–2963.

7. Dupont Y, Gabriel A, Chabre M, Bulik-Krzywicki T, Schecter E. Use of a new detector for X-ray diffraction and kinetics of the ordering of the lipids in *E. coli* membranes and models. Nature 1972;238:331–333.

8. Gabriel A, Dupont Y. A position sensitive proportional detector for X-ray crystallography. Rev Sci Instrum 1972;43:1600–1602.

9. Borkowski CJ, Kopp MK. Some applications and properties of one- and two-dimensional position-sensitive proportional counters. IEEE Trans Nucl Sci 1970;17:340–349.

10. Borkowski CJ, Kopp MK. Proportional counter photon camera. IEEE Trans Nucl Sci 1972;19:161–168.

11. Elsner G, Riekel C, Zachmann HG. Synchrotron radiation in polymer science. Adv Polym Sci 1985;67:1–58.

12. Elmore D, Tsao M, Chase B, Rabolt J. Planar array infrared (PAIR) spectrograph that operates in the 3400 to 2000 cm^{-1} region. Appl Spectrosc 2002;56:145–149.

13. Pellerin C, Snively C, Liu Y, Chase DB, Rabolt JF. Performance and application of a new planar array infrared spectrograph operating in the mid-infrared (2000–975 cm^{-1}) fingerprint region. Appl Spectrosc 2004;58:639–646.

14. Pellerin C, Frisk S, Rabolt JF, Chase DB. A faster approach to infrared rheo-optics using a planar array infrared spectrograph. Appl Spectrosc 2004;58:799–803.

15. Pearce R, Vancso GJ. Imaging of melting and crystallization of poly(ethylene oxide) in real-time by hot-stage atomic force microscopy. Macromolecules 1997;30:5843–5848.

16. Pearce R, Vancso GJ. Real-time imaging of melting and crystallization of poly(ethylene oxide) by atomic force microscopy. Polymer 1998;39:1237–1243.

17. Schultz JM, Miles MJ. AFM study of morphological development during the melt-crystallization of poly(ethylene oxide). J Polym Sci Polym Phys Ed 1998;36:2311–2325.

18. McMaster TJ, Brayshaw DJ, Miles MJ, Walsby AE, Dunton PG. A new ultra high speed AFM technique for biophysics: 3-dimensional imaging of surfaces, molecules and processes with true millisecond resolution. Biophys J 2005;88:541A.

19. Hobbs JK, Vasilev C, Humphris ADL. Real time observation of crystallization in polyethylene oxide with video rate atomic force microscopy. Polymer 2005;46:10226–10236.

20. Picco LM, Ulcinas A, Engledew DJ, Antognozzi M, Miles MJ. Video rate AFM for the real time characterisation of polymers and biological systems. Nano-molecular analysis for emerging technologies II, NMAETII; 2006 Oct 17–18; Teddington, UK; (2006).

21. Hobbs JK, Vasilev C, Humphris ADL. Video AFM – A new tool for high speed surface analysis. Analyst 2006;131:251–256.

22. Sun G, Weng L-T, Schultz JM, Chan C-M. Formation of banded and non-banded poly(L-lactic acid) spherulites during crystallization of films of poly(L-lactic acid)/poly(ethylene oxide) blends. Polymer 2014;55:1829–1836.

23. Cong Y, Hong Z, Qi Z, Zhou W, Li H, Liu H, Chen W, Wang X, Li L. Conformational ordering in growing spherulites of isotactic polypropylene. Macromolecules 2010;43:9859–9864.

24. Hay IL, Keller A. Polymer deformation in terms of spherulites. Kolloid-Z u Z Polymere 1965;204:43–74.

25. Kargin VA, Tsarevskaya IY. Deformation of crystalline polybutylene. Polym Sci U.S.S.R. 1996;13:1601–1607.

26. Erhardt P, Stein RS. A technique for the study of spherulite deformation: Light scattering movies. J Polym Sci 1965;3B:553–555.

27. Cowking A, Rider JG, Hay IL, Keller A. A study on the orientation effects in polyethylene in the light of crystalline texture. J Mater Sci 1968;3:646–654.

28. Cowking A, Rider JG. On molecular and textural reorientations in polyethylene caused by applied stress. J Mater Sci 1969;4:1051–1058.

29. Sakaoku A, Peterlin A. Bond rupture in highly oriented crystalline polymers. J Polym Sci 1969;7A-2:1151–1163.

30. Schultz JM. *Polymer Materials Science*. Englewood Cliffs, NJ: Prentice-Hall; 1974. , Chapter 11.

31. Stribeck N, Nöchel U, Funari SS, Schubert T. Tensile tests of polypropylene monitored by SAXS: Comparing the stretch-hold technique to the dynamic technique. J Polym Sci Polym Phys 2008;46:721–726.

32. Stribeck N, Nöchel U, Funari SS, Schubert T, Timmann A. Nanostructure of polypropylene in dynamic mechanical tests. Polym Chem Phys 2008;209:1992–2002.

33. Stribeck N. Deformation behavior of nanocomposites studied by X-ray scattering: Instrumentation and methodology. In: Karger-Kocsis J, Fakirov S, editors. *Nano- and Micro-Mechanics of Polymer Blends and Composites*. Munich, Germany: Carl Hanser Verlag; 2009. p 269–300.

34. Davies RJ, Zafeiropoulos NE, Schneider K, Roth SV, Burghammer M, Riekel C, Kotek JC, Stamm M. The use of synchrotron X-ray scattering coupled with in situ mechanical testing for studying deformation and structural change in isotactic polypropylene. Colloid Polym Sci 2004;282:854–866.

35. Davies RJ, Burghammer M, Riekel C. Simultaneous microfocus Raman and microfocus XRD: Probing the deformation of a single high-performance fiber. Macromolecules 2006;39:4834–4840.